

Nanoscale

Accepted Manuscript



This is an *Accepted Manuscript*, which has been through the Royal Society of Chemistry peer review process and has been accepted for publication.

Accepted Manuscripts are published online shortly after acceptance, before technical editing, formatting and proof reading. Using this free service, authors can make their results available to the community, in citable form, before we publish the edited article. We will replace this *Accepted Manuscript* with the edited and formatted *Advance Article* as soon as it is available.

You can find more information about *Accepted Manuscripts* in the [Information for Authors](#).

Please note that technical editing may introduce minor changes to the text and/or graphics, which may alter content. The journal's standard [Terms & Conditions](#) and the [Ethical guidelines](#) still apply. In no event shall the Royal Society of Chemistry be held responsible for any errors or omissions in this *Accepted Manuscript* or any consequences arising from the use of any information it contains.

Structure-induced Enhancement of Thermal Conductivities in Electrospun Polymer Nanofibers[†]

Cite this: DOI: 10.1039/x0xx00000x

Zhenxin Zhong,^{†a} Matthew C. Wingert,^{†b} Joseph Strzalka,^a Hsien-Hau Wang,^c Tao Sun,^a Jin Wang,^a Renkun Chen^{*b} and Zhang Jiang^{*a}

Received 00th January 2012,
Accepted 00th January 2012

DOI: 10.1039/x0xx00000x

www.rsc.org/

Polymers that are thermally insulating in bulk forms have been found to exhibit higher thermal conductivities when stretched under tension. This enhanced heat transport performance is believed to arise from the orientational alignment of the polymer chains induced by the tensile stretching. In this work, a novel high-sensitivity micro-device platform was employed to determine the axial thermal conductivity of individual Nylon-11 polymer nanofibers fabricated by electrospinning. Their thermal conductivity showed a correlation with the crystalline morphology measured by high-resolution wide-angle X-ray scattering. The relationship between the nanofiber internal structures and thermal conductivities could provide insights into the understanding of phonon transport mechanisms in polymeric systems and also guide future technical development of the fabrication and control of polymer nanofibers with extraordinary thermal performance and other desired properties.

Introduction

Recent progress in polymeric material engineering, especially in the synthesis and processing of materials with structure on nanometer-length scales, has created very promising opportunities for designing and fabricating a new class of nanostructured thermal transport materials with high thermal conductivity and compliant mechanical properties.^{1,2} It has been discovered that, in addition to enhanced mechanical performance,^{3,4} polymer materials under tension also exhibit increased thermal conductivity along the tensile direction.^{3,5-9} Polymeric materials, which are nearly insulating in bulk forms,¹⁰⁻¹² exhibit increased thermal conductivity when they are stretched to high draw ratios. For instance, the thermal conductivity (κ) of micron-sized polyethylene (PE) fibers was found to increase from 0.2 W/m-K in bulk forms to 50 W/m-K after drawing, accompanied by an increase in Young's modulus.³ More recently, Shen *et al.*¹ observed thermal conductivity as high as ~100 W/m-K for a single PE nanofiber (drawn from a gel to a diameter of ~100 nm). Polymer nanofibers therefore represent a new class of materials potentially suited to thermal applications and related technologies that require good thermal conductivity, electric insulation, mechanical flexibility, chemical stability, and other attributes uniquely related to polymers.

Heat transport mechanisms in polymers have been studied quite extensively. As an intrinsically low-dimensional system, isolated individual polymer chains can, in principle, have very high thermal conductivity.¹³ However, a macroscopic ensemble

of polymer chains is often a thermal insulator because of the twisted random orientations of the polymer chains and the weak coupling between the chains, in addition to inherent defects such as voids, impurities, polymer chain ends, and entanglements. These imperfections and defects generate high interfacial thermal resistance between conducting crystalline domains because high-frequency phonon modes within the crystalline domains must transfer to low-frequency modes across the domains. In highly stressed nanofibers, however, voids and entanglements are less likely to exist and polymer chains tend to form highly oriented structures as a result of transverse axial confinement and large surface aspect ratio. Molecular dynamic simulations have shown that κ of PE polymer nanofibers may achieve ~350 W/m-K,¹⁴⁻¹⁶ and is ever diverging with length.^{14,17,18}

These prior experimental and computational studies suggest a correlation between structures (e.g., crystalline domain size and orientation) and thermal conductivities in polymeric materials. In mechanical drawing experiments,^{1,3,5,8,19} it was believed that stress imposed during the fiber drawing re-orientes the crystallites along the draw direction. These crystallites are connected by tie-molecules that originate in the unfolding polymer chains. Upon further drawing, the number of fully extended tie-molecules increases, producing oriented and stretched polymer chains as well as increased crystal sizes, thereby enhancing mechanical strength and thermal conductivity. Much effort has therefore gone into developing advanced fabrication techniques, for example, direct proximal probe-based drawing¹ and nanoporous template wetting,²⁰ as

well as into uniaxially stretching bulk polymers into nanofibers of aligned chains in order to produce high modulus and high thermal conductivity.

Despite these recent advancements in thermal conductivity enhancement via drawing, there is still a lack of fundamental understanding of the relationship between the structures and attained thermal transport properties in polymer nanofibers. For instance, there is no study revealing how the size and anisotropic alignment of polymer crystallites is correlated with thermal transport. To that end, we used high-resolution in situ wide-angle X-ray scattering (WAXS) to systematically determine the structures of Nylon-11 nanofibers fabricated by electrospinning, which is a simple and versatile method to produce polymer nanofibers with controlled fiber diameters from tens of microns to tens of nanometers.²¹ Nylon-11 is a widely used polymer material in high-performance applications, and it is relatively easier to produce highly aligned Nylon-11 nanofibers through electrospinning. A highly sensitive micro-device platform was employed to measure the thermal conductivities of corresponding individual nanofibers. Using electrospun Nylon-11 as a model system, we established a close correlation between the axial thermal conductivity and crystalline structures (e.g., the orientational distribution and dimension of the crystallites). The methodology in the current study can be readily extended to other commonly investigated polymer materials, such as PVDF (polyvinylidene fluoride), PE, PEO (polyethylene glycol), and etc.

Results and discussion

Structural characterization

During the fast electrospinning, long filaments of Nylon-11 chains are wound up at an extremely high speed to form crystalline lamellar domains whose orientation and crystallization occur in line with the elongation flow along the extrusion direction. In each domain, the extended parallel chains are connected by hydrogen bonds forming a layered structure.^{22,23} These oriented crystallites are connected by networks of more disordered tie molecules or chain segments that represent the amorphous constituent of the internal structure. The mixed phase, consisting of co-existing amorphous and oriented crystalline regions and schematically shown in Fig. 1a, is confirmed by the WAXS pattern from uniaxially aligned as-spun Nylon-11 nanofibers where Bragg diffractions appear as broken arcs while the amorphous phase scatters X-rays to form a broader circular ring (Fig. 1b and 1c).

It is known that Nylon-11 possesses at least five different polymorphs depending on its method of preparation: the triclinic α -form, the monoclinic β -form, and three hexagonal or pseudo-hexagonal forms (γ , δ and δ' -forms).^{24,25} For example, isothermal crystallization of Nylon-11 from the melt and solution casted films from diols gives the triclinic α -form,²⁴ while crystals of β -form were reported obtaining from a solution of Nylon-11 in water containing 5% formic acid.²³ For both α and β -forms, two strong characteristic diffractions

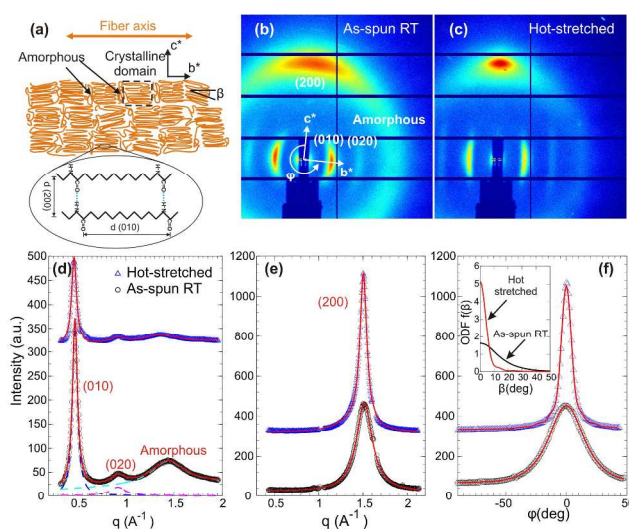


Fig. 1 (a) Schematic of the molecular arrangement in Nylon-11 nanofibers. WAXS patterns from uniaxially aligned nanofibers of an initial diameter of ~ 200 nm are shown for (b) as-spun at room temperature (RT) and (c) after hot-stretching to a $1.5\times$ draw ratio at 120°C , respectively. The long axis of the nanofibers are laid along the c^* axis, and the X-ray is incident perpendicular to the fibers (into the page). (d), (e) and (f) correspond to the intensity line cuts along (010) direction (b^* axis), (200) direction (c^* axis), and polar angle φ across the (200) diffraction peak, respectively. Solid red lines are fits to the models described in the text. Hot-stretched data are shifted vertically for clarity. Dashed blue, violet, and cyan curves displayed in (d) are best fits to the (010), (020), and amorphous peaks for the RT data, respectively. Inset in (f) shows corresponding orientational distribution functions of the crystalline domains as a function of inclination angle β of crystalline domain with respect to the nanofiber axis.

appear with d spacing 4.4 \AA and 3.7 \AA .^{22,23} There are also two other diffractions at 11.3 \AA and 14.9 \AA for α and β -forms, respectively, corresponding to the repeat unit of unit cell along the chain axis.^{22,23} The γ -form observed first on films cast from trifluoroacetic acid solution showed only one strong diffraction at 4.16 \AA .²⁶ Nylon-11 obtained by uniaxial stretching and electrospinning was also reported to produce γ -form with a strong X-ray diffraction at 4.1 \AA .²⁷ It has been shown that uniaxial deformation of Nylon-11 films can induce α - γ phase transition, yielding a γ -form dominant phase at the end of stretching with two strong diffraction peaks at 4.1 \AA and 14.0 \AA on the meridian and equator, respectively, the latter along stretched chain axis.²⁸ The γ -form is stable against heat treatment, and can be converted to the α -form by stretching, or melting and subsequent crystallization.^{26,29} Reversible α - δ transition was observed to occur at 95°C .³⁰ Nylon-11 quenched from the melt gives δ' -form with a single strong broad diffraction at 4.1 \AA .^{24,29} Annealing at a temperature higher than 95°C again converts the δ' -form to the α -form.^{24,29} In our study, strong diffractions at ~ 4.2 \AA and ~ 13.8 \AA (and its multiple),

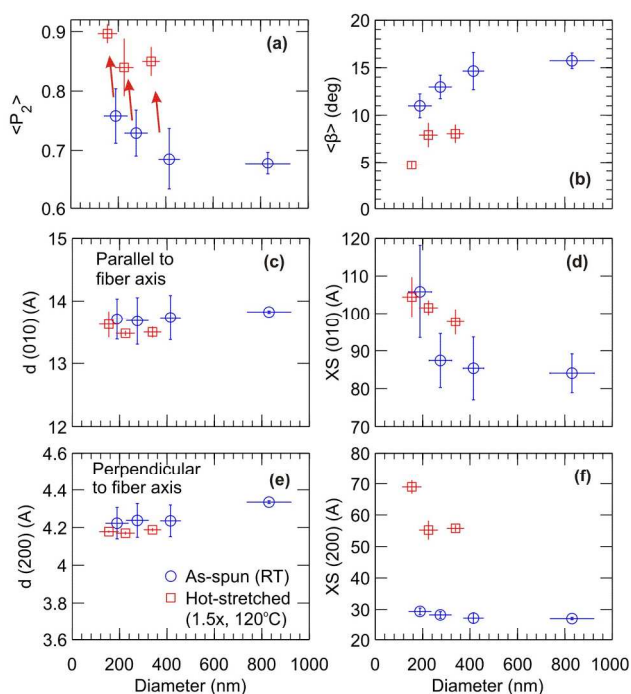


Fig. 2 Structure data of the crystalline domains as a function of diameter for nanofibers as-spun at room temperature (blue circles) and hot-stretched at 120°C to a 1.5× draw ratio (red squares). (a) and (b) are the orientational order parameter and average inclination angle, respectively; (c) and (e) are lattice parameters along the (010) direction (nanofiber axis) and (200) direction (perpendicular to nanofiber axis), respectively; (d) and (f) are the average crystalline domain sizes along the (010) and (200) directions, respectively. Error bars are standard deviations from measurements on multiple and identical nanofiber samples.

corresponding to the (200) (hydrogen bond direction) and the (010) (chain axis) diffractions of the γ -form (following the conventional selection of unit cell proposed by Kawaguchi *et al.*²³), were observed in as-spun Nylon-11 nanofibers electrospun from their hexafluoroisopropanol solutions (Fig. 1b and 1c). The γ -form crystals in electrospun Nylon-11 nanofibers were stable upon thermal treatment, which is consistent with those reported the literature,^{24,29} and we did not observe phase transition during the hot-stretching.

Detailed information about the internal structure can be obtained by quantitative analysis of the line shapes of the Bragg diffractions. The longitudinal (axial) line cut along the fiber b^* axis is excellently described by the superposition of the (010), (020) and the diffuse peak from the amorphous regions, which is modeled by three Lorentzian functions (Fig. 1d). The lattice spacing along the fiber axis can then be determined from the peak position, and the size of the crystalline domain is estimated from the peak width via the Scherrer equation.³¹ The shape factor of the amorphous phase obtained from the axial line cut is then used as the background scattering to extract the lattice spacing and crystalline domain dimension along the fiber

perpendicular direction c^* (Fig. 1e). The degree of the uniaxial orientational order of the crystalline domains is described by the orientational distribution function (ODF) $f(\beta)$, where β denotes the inclination angle between the long molecular chain axis and the fiber axis. The ODF can be obtained from the angular intensity distribution^{32,33} across the (200) Bragg peak, as shown in Fig. 1f. Knowing the ODF, any averaged orientational property $\langle X \rangle$ can be numerically calculated by

$$\langle X \rangle = \frac{\int_0^{\pi/2} X f(\beta) \sin \beta d\beta}{\int_0^{\pi/2} f(\beta) \sin \beta d\beta}. \quad (1)$$

In particular, the average inclination angle of the crystalline domains $\langle \beta \rangle$ and the 2nd-order orientational order parameter $\langle P_2 \rangle$ with respect to the fiber axis are determined by substituting X by β and $(3 \cos^2 \beta - 1)/2$, respectively. It should be noticed that the orientation due to the inter-fiber alignment in a bundle also contributes to the overall orientational WAXS analysis as a convolution with the intrinsic orientation arising from the molecular alignment.³⁴ Analysis on the scanning electron microscope (SEM) images, however, revealed that nanofibers are highly aligned so that the effect due to fiber alignment is very small in comparison to that from the intrinsic internal crystalline orientation (Supplementary Information Sec. 7). Quantitative structure information about the internal structures is summarized in Fig. 2 for as-spun and hot-stretched nanofibers as a function of nanofiber diameter, and will be discussed along with their thermal properties. The d -spacings of the (200) and (010) diffractions correspond to the γ -form and barely change for all the nanofibers in this study; their effect on thermal conductivity, therefore, will be ignored in the following discussions.

Size dependence of thermal conductivity

Stretching crystalline polymer films and fibers has been reported in both computer simulations and experiments to be capable of modifying crystalline structures or inducing crystal transitions, which subsequently can lead to enhanced or even new performance in mechanical and thermal properties.^{1,35,36} Although it has been recently proposed that the orientations of the amorphous phase would be responsible for some unexpected properties of the fibers when reducing their diameters,^{2,25,37} our WAXS data as the fibers were drawn was dominated by the evolution of the crystalline structures so the data statistics (Supplementary Information Sec. 9) did not reveal the improvement of the orientational distribution of the amorphous chains. It is commonly believed that drawing stretches the loose chains between crystal domains and yields increased tension in these chains and larger crystal size; on the other hand, the entangled polymer chains are restricted and the molecules orient themselves along the fiber axis direction, resulting in improved orientation. In the case of lamellar-structured Nylon-11, drawing can also enable the hydrogen-bonded polyamide sheets to slip past each other and form a more oriented structure.³⁸ The as-spun nanofibers are intrinsically highly stretched with an extremely high draw-ratio of 10^4 - 10^5 from the electrospinning process.³⁹ By uniaxially

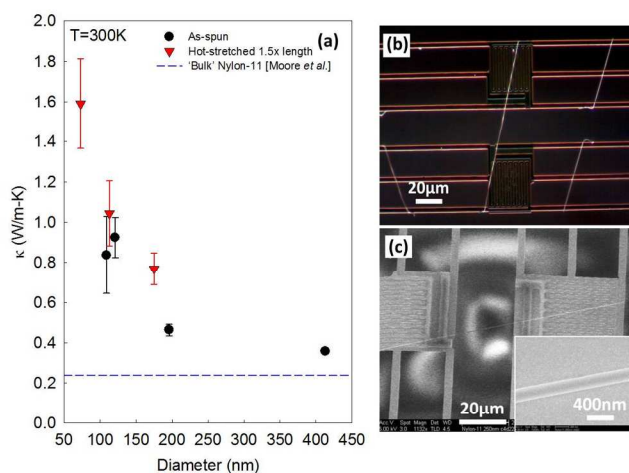


Fig. 3 (a) Thermal conductivity versus nanofiber diameter at 300 K. Black circles represent as-spun nanofibers and red triangles represent nanofibers hot-stretched to 1.5 \times original length. Thermal conductivity of all samples increases as diameter decreases, with larger increases among hot-stretched fibers. Blue dashed line represents bulk Nylon-11 values.¹⁰ (b) Dark-field optical image of nanofibers on a suspended micro-device for thermal measurement. (c) SEM of the same fiber in (b) with inset of a close-up of the fiber segment on the supporting pad.

drawing the as-spun nanofibers at elevated temperatures below Nylon-11's melting point ($T_m=198^\circ\text{C}$), we succeeded in obtaining an extra draw ratio of up to 2 \times original length. Data with a draw ratio of 1.5 \times were demonstrated in this study as the 1.5 \times ratio is applicable for all fibers. The structural improvements and the tension along the polymer chains are expected to increase the axial thermal conductivity, which was indeed observed in the present study.

Fig. 3a shows the increasing axial thermal conductivity κ measured at room temperature on as-spun and hot-stretched Nylon-11 nanofibers as a function of fiber diameter. As-spun nanofibers, even the one with 413-nm diameter, displayed a higher thermal conductivity than the literature values (0.216–0.24 W/m-K) of bulk Nylon-11,^{10,40,41} and the thermal conductivity increased as fiber diameter was further reduced to 196 nm, 121 nm, and 109 nm. Hot-stretched nanofibers (175 nm, 113 nm, and 73 nm) had even higher thermal conductivity values than those of similarly sized as-spun samples. Due to the challenging nature of the thermal conductivity measurements of individual nanofibers, it was prohibitively time-consuming to carry out these measurements with a broad sampling to probe possible variations of thermal properties of fibers with the same diameter. Such a study with large sampling size would be useful to establish a stronger diameter-dependence correlation, which warrants more systematic experimental study in the future.

As-spun nanofibers The increase in thermal conductivity with decreasing diameter for as-spun nanofibers is strongly

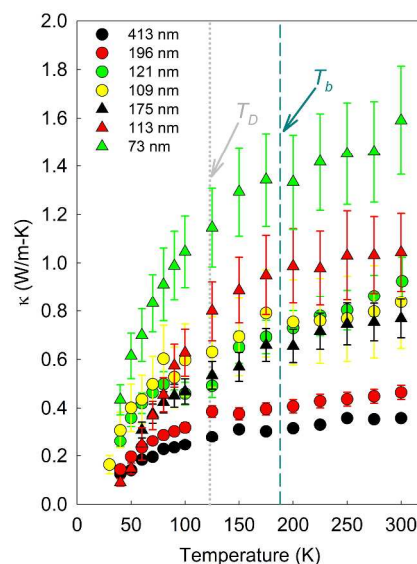


Fig. 4 Thermal conductivity versus temperature for all measured nanofiber samples. Nanofiber diameters ranged from the largest at 413 nm down to the smallest at 73 nm. Fibers of diameters 413, 196, 121, and 109 nm (circles) were as-spun, whereas the 175, 113, and 73 nm diameter fibers (triangles) were hot-stretched to 1.5 \times original length. Vertical lines denote Debye (T_D) and brittleness (T_b) temperatures for bulk Nylon.

correlated with the structural trend revealed by the WAXS data (Fig. 2). The perpendicular crystal size, i.e., along the (200) direction, does not vary as the fiber diameter reduces from the micron scale to ~ 200 nm (Fig. 2f), while the longitudinal crystal size grows by $\sim 25\%$ (Fig. 2d), implying a longer phonon mean free path (MFP) along the aligned molecular chains before phonons are scattered at crystal boundaries. Moreover, the population fraction of crystals whose extended chains are parallel to the fiber axis is higher as the fiber diameter decreases, which has been verified by the higher orientational order parameter $\langle P_2 \rangle$ and smaller averaged crystal inclination angle $\langle \beta \rangle$ (Fig. 2a and 2b). This further facilitates phonon propagation along the fiber axis. On the other hand, the crystallinity analysis⁴² reveals a nearly constant degree of crystallinity of 36% for all the studied nanofibers (Supplementary Information Sec. 10), consistent with 35–45% determined by X-ray diffraction and differential scanning calorimetry on electrospun Nylon nanofibers^{11,43} and bulk Nylon samples.^{44,45} In addition, WAXS from bulk Nylon-11 samples does not reveal preferred orientations (Supplementary Information Sec. 8). Therefore, it is the improved crystallite orientation and polymer chain alignment arising from the confinement of diameter reduction rather than the fraction of crystallinity that contributes to the enhanced thermal performance.

Hot-stretched nanofibers As the diameter reduces below a critical value of ~ 200 nm, regardless of as-spun or hot-stretched nanofibers, κ increases in an accelerated trend (Fig. 3a),

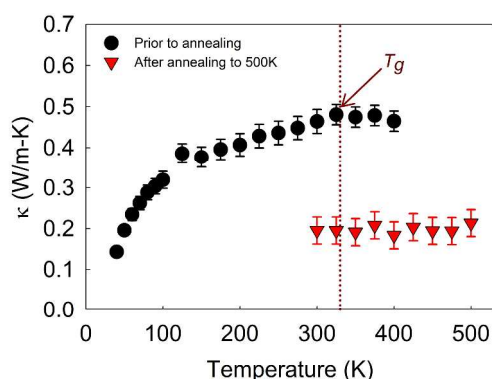


Fig. 5 Thermal conductivity versus temperature for annealed nanofiber sample NF2 (196 nm diameter as-spun). Nanofiber thermal conductivity was measured from 30 K to 400 K (black circles) and further annealed to 500 K. The thermal data above room temperature shows a peak at ~ 330 K, which is approximately the glass transition temperature for Nylon (vertical dotted line). After holding at 500 K for ~ 1 hr, the sample was cooled to room temperature and the thermal conductivity was re-measured from 300 K to 500 K (red triangles) and found to be significantly reduced.

consistent with previous studies on PE nanofibers,^{1,3} albeit with lower κ for the stretched Nylon fibers studied herein. In addition, hot-stretched nanofibers show higher κ values than as-spun fibers with comparable diameters. This enhancement is correlated with the in situ hot-stretching WAXS data, which reveal a significantly narrower orientational distribution of the crystals, i.e., $\langle P_2 \rangle$ increased from 0.75 for as-spun 190-nm nanofiber to 0.9 after hot-stretching (Fig. 2a), and the averaged crystal inclination angle reduced from 11° to 4.4° (Fig. 2b). In contrast to a very small change in the longitudinal crystal size, the transverse crystal size after hot-stretching expanded to more than twice that of the as-spun fibers, which implies a much lower phonon scattering probability at the crystal boundaries and hence an increase in thermal conductivity along the crystal axis. For the smallest hot-stretched nanofiber in the present study (73 nm in diameter), the thermal conductivity is about 1.6 ± 0.2 W/m-K, more than $6\times$ that of bulk Nylon.

It is also worth pointing out that the conductivities of the hot-stretched fibers, regardless of the size, are consistently slightly higher than those of the as-spun fibers. As can be seen from Fig. 3a, the hot-stretched 113nm fiber has a higher thermal conductivity than the 121nm and 109nm as-spun fibers. This observation indicates that the stretching leads to higher orientation order in addition to the effect of the diameter reduction.

Temperature dependence of thermal conductivity

To further understand phonon scattering mechanisms in nanofibers, we investigated the temperature dependence of κ over a temperature range of 30-300 K. Bulk Nylon exhibits three temperature regimes: 1) below the Debye temperature T_D ,

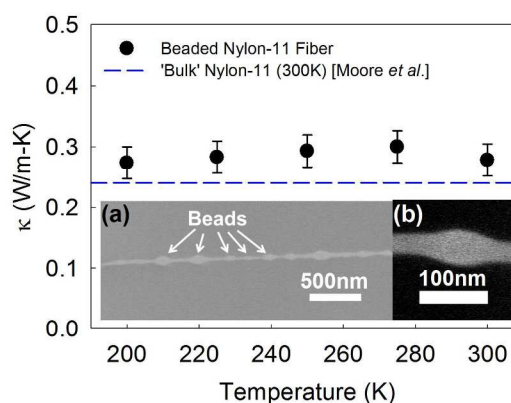


Fig. 6 Thermal conductivity of a beaded nanofiber. Bulk Nylon-11¹⁰ (blue dashed line) shown for comparison purposes. Inset (a) shows an SEM image of a beaded nanofiber segment with several beaded structures marked. Inset (b) shows an individual bead structure from the beaded fiber.

2) above the Debye temperature but below the brittleness temperature T_b , and 3) above the brittleness temperature up to room temperature. The temperature dependence of thermal conductivity can be understood from the relation, $\kappa \propto Cv_l$, where C is the heat capacity, v is the phonon speed of sound, and l is the phonon MFP. In the first regime, the temperature dependence is due to the increase in heat capacity with increasing temperature which saturates approaching the Debye temperature. In the second regime, the heat capacity is constant, but there is still a slight increase in κ , up to the brittleness temperature (~ 188 K⁴⁶). Above T_b , in the third regime, κ is nearly constant. This provides a baseline for comparison with the measured nanofibers.

In the first regime, below T_D (~ 123 K for bulk Nylon-11⁴⁷), the temperature dependence is again due to the heat capacity, however, the κ increase is scaled higher at smaller diameters due to longer phonon MFPs from the increased crystal size and orientation. The thermal conductivity, however, increases above the bulk Debye temperature, which becomes more pronounced for smaller diameter fibers. This is possibly due to the relationship between the Debye temperature and the elastic modulus, E , ($T_D \propto \sqrt{E}$),⁴⁸ where increasing E with decreasing diameter² leads to increases in T_D for smaller nanofibers. This could be the reason there is no discernable plateau or maximum in the thermal conductivity over the measured temperature range.

Impurity and inter-chain scattering dominates thermal transport in bulk and amorphous Nylon.¹¹ Similar scattering mechanisms also exist in the nanofibers in the present study, but with reduced impurity and inter-chain scattering leading to the higher κ . Moreover, a recent study⁴⁹ on the thermal conductivity of polymers has seen $1/T$ temperature dependence above the peak in κ due to Umklapp scattering. However, these polymers had a crystallinity of $\sim 80\%$, whereas the Nylon in this study is comparatively low at $\sim 36\%$, leaving much of the

polymer amorphous. This large amorphous component could reduce the peak thermal conductivity and mask the $1/T$ behaviour in the measured κ data.

High temperature measurement and annealing effect

The thermal properties were also examined on an as-spun nanofiber sample (196 nm in diameter) above room temperature before and after annealing at 500 K (Fig. 5). In the heating cycle before the annealing, κ maximizes at ~ 330 K, around Nylon's glass transition temperature (325-335 K),^{50,51} and declines again upon further temperature increase. Similar behavior has been previously observed in some other polymers.^{49,51} As the temperature rises above the glass transition temperature, structural changes⁵² cause a decrease in κ .⁴⁹ The nanofiber was then annealed at 500 K (slightly above the T_m of 471 K) for about one hour without breaking the fiber and then allowed to cool to room temperature; its conductivity was found to be significantly depressed from 0.48 to 0.19 W/m-K at ~ 330 K. This may be accounted for by a few possible changes of the internal structures which were challenging in the current study to identify on single free-standing fibers: the degree of crystallinity substantially decreased; crystal size and morphology may be significantly affected; or more probably, preferred molecular orientation of the crystallites with respect to the fiber axis was lost with the thermal history.

Effects of structural defects

The close correlation between structural and thermal properties in electrospun nanofibers was also clearly demonstrated in a nanofiber with intentionally induced defects, namely, a beaded nanofiber (Fig. 6). The capillary instability squeezes the fluid electrospinning jet into droplets that are still connected by the entangled polymer chains, thereby forming a beaded structure.⁵³ Previous orientation analysis along single-beaded fibers via electron diffraction has revealed a bulk-like structure in the beads with randomly oriented crystallites,⁵⁴ which can account for the measured bulk-like κ (~ 0.28 W/m-K) for the beaded nanofiber in the present study (details of κ calculation in Supplemental Information Sec. 5).

Comparison with other nanofibers

In agreement with Shen *et al.*,¹ our results showed a significant structural-induced increase in thermal conductivity in small diameter nanofibers. The lower absolute κ observed in the Nylon-11 nanofibers as compared to PE, is attributed to the intrinsic difference in the molecular structure and the lower crystallinity. In addition, the macroscopic conductivity of an ensemble of polymer chains drastically depends on the manner in which the chains are folded. Linear high-density PE has the simplest molecular structure with chains that can fold to form almost entirely crystalline domains (80-90% crystallinity)³ with a much higher packing density than its amorphous counterpart. In contrast, the degree of crystallinity of Nylon-11 is only 35-40%, leaving most of the polymer in non-crystalline phase with

very high thermal resistance. Furthermore, both experimental studies on PE mats⁵ and molecular simulations on individual polymer chains^{18,55,56} have shown that polymers of high mechanical strength also have superior thermal performance. Given Nylon's intrinsically lower Young's modulus (~ 25 GPa) of the crystalline lattice compared to PE (~ 240 GPa),⁵⁷ it is expected to possess a much lower thermal conductivity.

The structural properties and corresponding enhanced thermal conductivities of the Nylon nanofibers in the present study correlate well with their mechanical properties previously studied. As the electrospun nanofiber diameter reduces to 200-500 nm, it has been shown to exhibit rapidly rising Young's modulus and ultimate tensile strength along the fiber axis.⁴ The fast electrospinning induces tensile strains on polymer chains even in the amorphous region. This lowers the phonon-phonon scattering and improves energy transport along the polymer backbones.³¹

Conclusions

We have established a relationship between the internal crystalline structures of electrospun Nylon-11 nanofibers with high as-spun draw ratio and their axial thermal properties. In consistence with previous experimental studies,^{1,3,6} we found that although the thermal conductivity starts deviating from the bulk value when the fibers reach as thick as several hundred nanometers (e.g. ~ 400 nm), this further accelerates only when the nanofiber diameter decreases to about two hundred nanometers, where crystallites start to show a significantly higher degree of preferred orientation with respect to the fiber axis. The combination of crystal size growth and improved orientational order (along with the narrowing of crystalline domain inclination distribution) increases the intermediate-range order and the phonon MFP, resulting in an enhanced thermal conductivity. Additional axial hot-stretching improved the orientation distribution and the crystallite size, thereby further reducing phonon scattering at crystal boundaries and facilitating heat transport along the fibers. Subsequently, thermal conductivity six times greater than bulk was achieved on the thinnest Nylon nanofibers in the present study. It was a challenge to determine the crystalline structures of the thinnest fibers (<100 -200 nm in diameter) because of the difficulty of collecting high-quality ultrathin nanofiber bundles for WAXS measurements. However, the trend observed for larger fibers has unambiguously suggested a positive correlation between the crystalline structure and thermal conductivity in electrospun nanofibers. It is therefore believed that even higher thermal performance might be achieved if crystalline structure gets further improved as the nanofiber diameter further reduces.

Temperature-dependent tests showed some deviation from bulk behavior below room temperature. The larger crystal size increased thermal conductivity over the entire temperature range. This would plateau near the Debye temperature, which could shift to higher temperature with decreasing fiber diameter. On the other hand, increasing temperature above T_g led to a maximum thermal conductivity around T_g . It was also

found from the beaded fibers that the disordering in crystallite orientations as well as nanofiber defects can significantly reduce the thermal conductivity to close to bulk-like values.

Nylon-11 is a ferroelectric polymer⁵⁸ and the dipole interactions can help improve the crystallite orientations during the electrospinning, as have been observed in other ferroelectric polymers such as PVDF.⁵⁹ The effect of the ferroelectricity of polymer nanofibers on their thermal behavior is certainly of great interest for future investigations, yet there is no direct evidence on their correlations. Since the main set of thermal measurements were conducted below the glass transition temperature of Nylon-11 (between 40-70°C),⁵¹ ferroelectric effects should be negligible. In addition, for measurements above the transition temperature, electronic contributions to the thermal conductivity are negligible and dominated by phonon transport.

In summary, our findings from the Nylon-11 nanofibers provided very important experimental evidence of the dependence of the thermal performance on the crystalline morphology of the polymer nanofibers. Therefore, these studies will not only shed light on further understanding of phonon transport mechanisms in low-dimensional polymer systems, but also lay out a possible path to achieve full control of the design and fabrication of nanostructured polymer nanofibers endowed with high thermal conductivity and other desired properties.

Experimental section

Sample preparation

Nylon-11 pellets (Sigma-Aldrich) with a density of 1.026 g/mL (melting temperature $T_m=198^\circ\text{C}$) were dissolved in 1,1,1,3,3,3-Hexafluoro-2-propanol (HFIP, from Sigma-Aldrich). Solution concentration varied from 2 wt% to 12.5 wt% for the control of nanofiber diameters. The nanofibers were spun on a vertical electrospinning apparatus (Fig. S3) with an electric potential of 6-7 kV. In order to produce uniaxially aligned nanofibers, two parallel collecting electrodes were placed 20-30 cm below the spinneret.⁶⁰ The electrospinning jet then stretched itself across the gap as the electric field lines are attracted towards the edges of the electrode. The electrostatic repulsion between the deposited charged fibers further facilitated the parallel and relatively even distribution of fibers.^{61,62} The highly oriented nanofibers were then carefully transferred either onto micro-devices for thermal property measurement or to an X-ray-compatible vacuum chamber for internal structure characterization. The diameters of nanofibers were determined on an FEI Quanta 400F environmental scanning electron microscope (SEM).

Crystalline structural measurement

The internal crystalline structures of the nanofibers, in terms of lattice dimension, crystalline size, and orientational order, etc., were quantitatively characterized using wide-angle X-ray scattering (WAXS) at beamline 8-ID at the Advanced Photon Source with an X-ray energy of 7.35 keV.⁶³ The aligned

nanofibers were placed under tension between two parallel posts that can be individually translated axially in order to stretch the nanofibers. Controlled thermal annealing of the nanofibers was achieved via homogenous infrared radiation from an in-vacuum IR heater (200 W, 120 V, Mor Electric Heating Assoc., Inc., USA). *In situ* hot-stretching was performed by ramping to and maintaining the desired annealing temperature until fibers reached structural equilibrium, followed by uniaxial stretching at a rate of 5 $\mu\text{m/s}$. The temperature was measured with a platinum resistance thermometer placed in close proximity to the nanofiber sample. To protect the polymer nanofibers from radiation damage, the samples as well as the entire hot-stretching instrument are enclosed in an X-ray compatible vacuum chamber. WAXS patterns were recorded by a single-photon-counting pixel array detector (Pilatus 1M, Dectris) located 194 mm downstream from the sample. Routine WAXS data processing was performed for air gap scattering, efficiency, polarization, and solid angle before the 2D WAXS data were finally reduced to 1D data for further data analysis.

Thermal measurement

The thermal conductivity of the Nylon-11 nanofibers was measured using the well-established suspended micro-device method^{64,65} over a wide temperature range. Pt resistance thermometer coils patterned onto suspended SiN_x membranes allow for heating and temperature sensing, where one coil acts as a heater to create a temperature differential across the individual nanofibers, and both coils simultaneously act as thermometers to measure the temperature rise of each suspended membrane. Measurements were performed in a vacuum chamber evacuated to better than $\sim 10^{-5}$ Torr to reduce the conduction and convection heat transfer due to residual air molecules. Heat loss along the suspending beams supporting the heating and sensing membranes as well as along the nanofiber was found to be within the systematic error of the nanofiber thermal property measurement and thereby can be negligible (Supplementary Information Sec. 3 and 4).

Excess nanofibers on the micro-devices were cut using focused ion beam (FIB) with care taken to avoid accidental Ga ion or electron beam damage⁶⁶ to the nanofiber of interest (Fig. 3b and 3c). Platinum deposition for enhanced thermal contact between nanofibers and SiN_x membranes was not applied as it was found to damage the fibers and reduce measured thermal conductivity values (Supplementary Information Sec. 1). The conductivity reported here therefore includes the thermal contact resistance, thereby representing the lower bound of the intrinsic value of the nanofibers. The contact resistance, however, is estimated to be very small compared to the fiber conduction resistance based on previous investigations on suspended nanowire/fiber systems (Supplementary Information Sec. 2).⁶⁷

Since the thermal conductance of thin polymer nanofibers herein is rather low compared to wires made of most inorganic materials, we employed a sensitive measurement technique

based on the Wheatstone bridge, which can resolve a thermal conductance as low as ~ 0.1 nW/K.⁶⁸ Our measurements suggested that the contribution from the background conductance is not negligible due to the low conductance of the nanofibers. Therefore, a ‘canceling’ scheme^{69,70} was applied so that the background is directly subtracted by measuring the conductance difference between a nanofiber device and a neighboring identical blank device with no nanofiber.

Acknowledgements

Work at Argonne National Laboratory, including the use of Advanced Photon Source and Electron Microscopy Center, Office of Use Office of Science User Facilities operated for the U.S. Department of Energy (DOE) Office of Science by Argonne National Laboratory, was supported under DOE contract DE-AC02-06CH11357. R.C. and M.C.W. acknowledge the support from the Thermal Transport Program of the National Science Foundation (CBET-1336428). The FIB work was performed at the Laboratory for Electron and X-ray Instrumentation (LEXI) at UC Irvine, using instrumentation funded in part by the National Science Foundation Center for Chemistry at the Space-Time Limit (CHE-082913).

Notes and references

^a X-ray Science Division, Argonne National Laboratory, Argonne, Illinois 60439, USA. Email: zjiang@aps.anl.gov

^b Department of Mechanical and Aerospace Engineering, University of California San Diego, La Jolla, California 92093, USA. Email: rkchen@ucsd.edu

^c Material Science Division, Argonne National Laboratory, Argonne, Illinois 60439, USA.

[†] Z.Z. and M.C.W. contributed to this work equally. Electronic Supplementary Information (ESI) available: E-beam platinum bonding induced damage, estimation of contact resistance between nanofibers and suspended pads, effects of heat loss from suspended devices, estimation of heat loss along nanofiber, diameter calculation for beaded fiber, schematics of electrospinning and WAXS setup, orientation analysis of the inter-fiber alignment, WAXS patterns from bulk samples, WAXS data analysis strategy, and estimation of the crystallinity. See DOI: 10.1039/b000000x/

- 1 S. Shen, A. Henry, J. Tong, R. T. Zheng and G. Chen, *Nat. Nanotechnol.*, 2010, **5**, 251.
- 2 A. Arinstein, M. Burman, O. Gendelman and E. Zussman, *Nat. Nanotechnol.*, 2007, **2**, 59.
- 3 C. L. Choy, Y. W. Wong, G. W. Yang and T. Kanamoto, *J. Polym. Sci. Pol. Phys.*, 1999, **37**, 3359.
- 4 C. T. Lim, E. P. S. Tan, S. Y. Ng, *Appl Phys Lett* **2008**, **92**, 141908.
- 5 T. Kanamoto, A. Tsuruta, K. Tanaka, M. Takeda and R. S. Porter, *Macromolecules*, 1988, **21**, 470.
- 6 D. B. Mergenthaler, M. Pietralla, S. Roy and H. G. Kilian, *Macromolecules*, 1992, **25**, 3500.
- 7 B. Poulaert, J. C. Chielens, C. Vandenhende, J. P. Issi and R. Legras, *Polym. Commun.*, 1990, **31**, 148.
- 8 P. Smith and P. J. Lemstra, *J. Mater. Sci.* 1980, **15**, 505.
- 9 C. L. Choy, Y. Fei and T. G. Xi, *J. Polym. Sci. Pol. Phys.*, 1993, **31**, 365.
- 10 A. L. Moore, A. T. Cummings, J. M. Jensen, L. Shi and J. H. Koo, *J. Heat Trans.-T. Asme*, 2009, **131**, 091602.
- 11 C. L. Choy, E. L. Ong and F. C. Chen, *J. Appl. Polym. Sci.*, 1981, **26**, 2325.
- 12 G. DeCarvalho, E. Frollini and W. N. DosSantos, *J. Appl. Polym. Sci.*, 1996, **62**, 2281.
- 13 S. Lepri, R. Livi and A. Politi, *Phys. Rep.*, 2003, **377**, 1.
- 14 A. Henry and G. Chen, *Phys. Rev. Lett.*, 2008, **101**, 235502.
- 15 A. Henry, G. Chen, S. J. Plimpton and A. Thompson, *Phys. Rev. B*, 2010, **82**, 144308.
- 16 T. Zhang and T. Luo, *ACS Nano*, 2013, **7**, 7592.
- 17 A. Henry and G. Chen, *Phys. Rev. B*, 2009, **79**, 144305.
- 18 J. W. Jiang, J. H. Zhao, K. Zhou and T. Rabczuk, *J. Appl. Phys.*, 2012, **111**, 124304.
- 19 G. Capaccio and I. M. Ward, *Polym. Eng. Sci.*, 1975, **15**, 219.
- 20 B. Y. Cao, Y. W. Li, J. Kong, H. Chen, Y. Xu, K. L. Yung and A. Cai, *Polymer*, 2011, **52**, 1711.
- 21 D. H. Reneker and A. L. Yarin, *Polymer*, 2008, **49**, 2387.
- 22 S. Rhee and J. L. White, *J. Polym. Sci. Pol. Phys.*, 2002, **40**, 2624.
- 23 A. Kawaguchi, T. Ikawa, Y. Fujiwara, M. Tabuchi and K. Monobe, *J. Macromol. Sci. Phys.*, 1981, **B20**, 1.
- 24 Q. Zhang, Z. Mo, H. Zhang, S. Liu and S. Z. D. Cheng, *Polymer*, 2001, **42**, 5543.
- 25 M. Richard-Lacroix and C. Pellerin, *Macromolecules*, 2013, **46**, 9473.
- 26 T. Sasaki, *J. Polym. Sci. Part B: Polym. Lett.*, 1965, **3**, 557.
- 27 M. Dhanalakshmi and J. P. Jog, *EXPRESS Polym. Lett.*, 2008, **2**, 540.
- 28 S. Moffatt, A. Ajji, B. Lotz and J. Brisson, *Can. J. Chem.*, 1998, **76**, 1491.
- 29 P. K. Chen, B. A. Newman, J. I. Scheinbeim and K. D. Pae, *J. Mater. Sci.*, 1985, **20**, 1753.
- 30 B. A. Newman, T. P. Sham and K. D. Pae, *J. Appl. Phys.*, 1977, **48**, 4092.
- 31 J. I. Langford and A. J. C. Wilson, *J. Appl. Crystallogr.*, 1978, **11**, 102.
- 32 P. Davidson, D. Petermann and A. M. Levelut, *J. Phys. II.*, 1995, **5**, 113.
- 33 F. Giesselmann, R. Germer and A. Saipa, *J. Chem. Phys.*, 2005, **123**, 034906.
- 34 M. D. Edwards, G. R. Mitchell, S. D. Mohan and R. H. Olley, *Eur. Polym. J.*, 2010, **46**, 1175.
- 35 J. Liu and R. G. Yang, *Phys. Rev. B*, 2010, **81**, 174122.
- 36 S. Pal, G. Balasubramanian and I. K. Puri, *J. Chem. Phys.*, 2012, **136**, 044901.
- 37 D. Papkov, Y. Zou, M. N. Andalib, A. Goponenko, S. Z. D. Cheng and Y. A. Dzenis, *ACS Nano*, 2013, **7**, 3324.
- 38 J. W. S. Hearle and R. H. Peters, *Fibre structure*. Textile Institute: 1963.
- 39 A. L. Yarin, S. Koombhongse and D. H. Reneker, *J. Appl. Phys.*, 2001, **89**, 3018.
- 40 J. E. Mark, *Physical properties of polymers handbook*. 2nd ed.; Springer: New York, 2007.

- 41 J. F. Shackelford and W. Alexander, *CRC materials science and engineering handbook*, 3rd ed.; CRC Press: Boca Raton, FL, 2001.
- 42 N. S. Murthy and H. Minor, *Polymer*, 1990, **31**, 996.
- 43 C. Carrizales, S. Pelfrey, R. Rincon, T. M. Eubanks, A. X. Kuang, M. J. McClure, G. L. Bowlin and J. Macossay, *Polym. Advan. Technol.*, 2008, **19**, 124.
- 44 G. W. Ehrenstein and R. P. Theriault, *Polymeric materials: structure, properties, applications*. Hanser: Munich, 2001.
- 45 P. Ricou, E. Pinel and N. Juhasz, *Advances in X-ray Analysis* 2005, **48**, 170.
- 46 H. W. Starkweather and R. E. Brooks, *J. Appl. Polym. Sci.*, 1959, **1**, 236.
- 47 A. Xenopoulos and B. Wunderlich, *Polymer*, 1990, **31**, 1260.
- 48 M. X. Gu, C. Q. Sun, Z. Chen, T. C. Au Yeung, S. Li, C. M. Tan and V. Nosik, *Phys. Rev. B*, 2007, **75**, 125403.
- 49 X. J. Wang, V. Ho, R. A. Segalman and D. G. Cahill, *Macromolecules*, 2013, **46**, 4937.
- 50 T. Ashworth, L. R. Johnson, C. Y. Hsiung and M. M. Kreitman, *Cryogenics*, 1973, **13**, 34.
- 51 R. M. Neagu, E. Neagu, N. Bonanos and P. Pissis, *J. Appl. Phys.*, 2000, **88**, 6669.
- 52 P. Dashora and G. Gupta, *Polymer*, 1996, **37**, 231.
- 53 H. Fong, I. Chun and D. H. Reneker, *Polymer*, 1999, **40**, 4585.
- 54 T. Yoshioka, R. Dersch, M. Tsuji and A. K. Schaper, *Polymer*, 2010, **51**, 2383.
- 55 T. F. Luo, K. Esfarjani, J. Shiomi, A. Henry and G. Chen, *J. Appl. Phys.*, 2011, **109**, 074321.
- 56 T. F. Luo and J. R. Lloyd, *Adv. Funct. Mater.*, 2012, **22**, 2495.
- 57 I. Sakurada, T. Ito and K. Nakamae, *J. Polym. Sci. Pol. Sym.*, 1967, **15**, 75.
- 58 J. I. Scheinbeim, J. W. Lee and B. A. Newman, *Macromolecules*, 1992, **25**, 3729.
- 59 C.-C. Tsai, P. Mikes, T. Andruk, E. White, D. Monaenkova, O. Burtovyy, R. Burtovyy, B. Rubin, D. Lukas, I. Luzinov, J. R. Owens and K. G. Kornev, *Nanoscale*, 2011, **3**, 4685.
- 60 C. Lai, G. Zhong, Z. Yue, G. Chen, L. Zhang, A. Vakili, Y. Wang, L. Zhu, J. Liu and H. Fong, *Polymer*, 2011, **52**, 519.
- 61 D. Li, Y. L. Wang and Y. N. Xia, *Nano Lett.*, 2003, **3**, 1167.
- 62 S. Ramakrishna, *An introduction to electrospinning and nanofibers*. World Scientific: Hackensack, NJ, 2005.
- 63 Z. Jiang, X. Li, J. Strzalka, T. Sun, M. Sprung, A. Sandy, S. Narayanan, D. R. Lee and J. Wang, *J. Synchrotron Radiat.*, 2012, **19**, 627.
- 64 L. Shi, D. Y. Li, C. H. Yu, W. Y. Jang, D. Kim, Z. Yao, P. Kim and A. Majumdar, *J. Heat Trans.-T. Asme*, 2003, **125**, 881.
- 65 D. Y. Li, Y. Y. Wu, P. Kim, L. Shi, P. D. Yang and A. Majumdar, *Appl. Phys. Lett.*, 2003, **83**, 2934.
- 66 D. L. Vezie, E. L. Thomas and W. W. Adams, *Polymer*, 1995, **36**, 1761.
- 67 C. H. Yu, S. Saha, J. H. Zhou, L. Shi, A. M. Cassell, B. A. Cruden, Q. Ngo and J. Li, *J. Heat Trans.-T. Asme*, 2006, **128**, 234.
- 68 M. C. Wingert, Z. C. Y. Chen, S. Kwon, J. Xiang and R. K. Chen, *Rev. Sci. Instrum.*, 2012, **83**, 024901.
- 69 J. Zheng, M. C. Wingert, E. Dechaumphai and R. Chen, *Rev. Sci. Instrum.*, 2013, **84**, 114901.
- 70 A. Weatshers, K. Bi, M. T. Pettes and L. Shi, *Rev. Sci. Instrum.*, 2013, **84**, 084903.